Trees (2015) 29:1115–1126
DOI 10.1007/s00468-015-1191-6

ORIGINAL PAPER

XRCT images and variograms reveal 3D changes in wood density of riparian trees affected by floods

Juan Antonio Ballesteros-Cánovas[1,2] · Markus Stoffel[1,2] · Carolina Guardiola-Albert[3]

Received: 11 November 2014 / Revised: 12 March 2015 / Accepted: 18 March 2015 / Published online: 7 April 2015

Abstract
Key message **The extension of damage and anatomical changes in riparian trees after flood impact can be quantified with X-ray computed tomography and variogram analyses.**
Abstract This paper combines X-ray computed tomography (XRCT) images and variogram analyses to document the response of riparian trees to mechanical damage caused by floods. Changes in wood anatomy and density have been described in the past to occur as a result of severe cambial tissue damage. However, knowledge is still fragmentary insofar as the spatial extent of responses is concerned and in terms of causative factors controlling the magnitude of response. Here, we present a novel approach combining non-destructive XRCT images with geostatistical tools to describe the extension of anatomical changes in 30 specimens of 3 Mediterranean riparian species (*Alnus glutinosa* (L.) Gaertn., *Fraxinus angustifolia* Vahl. and *Salix atrocinerea* Brot.) scarred by floods. We visually assess tree and wound characteristics (i.e., wound size, decayed area, callus length, callus mark) as well as the health state of trees prior to wounding. In parallel, we systematically computed 1D variograms using XRCT images so as to quantify relative tangential changes in wood density after wounding. Based on non-parametric statistical tests and Principal Component Analyses (PCA), we identify possible controls of macroscopic anatomical features on tangential affected area (TAA) and decay processes. Reactions in trees are controlled differently between species, but are driven above all by the health state of the tree prior to wounding. In view of the expected increase in the frequency of hydrogeomorphic processes and/or changes in the availability of sediments in a future greenhouse climate, wounding of trees is expected to occur more frequently in riparian forests, which could have negative effects on the sustainability of riparian vegetation.

Keywords Cambial injury · Riparian trees · Wood density · XRCT images · Wood anatomy · Variogram · Wood analysis

Communicated by E. Liang.

✉ Juan Antonio Ballesteros-Cánovas
juan.ballesteros@dendrolab.ch

[1] Dendrolab.ch, Institute of Geological Sciences, University of Berne, 3012 Berne, Switzerland

[2] Climatic Change and Climate Impacts, Institute for Environmental Sciences, University of Geneva, 1227 Carouge, Switzerland

[3] Geological Survey of Spain (IGME), Ríos Rosas 23, 28003 Madrid, Spain

Introduction

Hydrological processes and related disturbance strongly influence the life cycle of riparian forests and modulate the establishment of new plants, their development as well as their mortality (Sigafoos 1964; Kozlowski 1997; Stoffel and Wilford 2012). Stem wounds in trees are one of the most obvious consequences that hydrological processes may have on vegetation. During floods, the interaction between sediment and woody debris typically favors the partial removal of the bark and, consequently a localized dysfunction of cambial tissues (Ballesteros et al. 2011a, b). After wounding, trees will suffer from the loss of structural capacity as well as from changes in their metabolism and hormonal growth (Dekhuijzen 1976; Lowerts and Kellison 1981), which in turn will render them more vulnerable to

pathogen invasion and related increase in mortality (Schweingruber et al. 2006).

After cambial damage, trees will produce cellular and chemical changes by forming "walls" around the wound so as to prevent embolism, pathogen infections, and decay processes in the healthy parts of the stem (CODIT concept, Compartmentalization of Decay in Trees; Shigo 1984). The most important macroscopic features described to occur after wounding (Smith and Sutherland 2001; Grünwald et al. 2002; Stobbe et al. 2002; Bollschweiler et al. 2008; Stoffel and Hitz 2008; Schneuwly et al. 2009a, b) include discolored xylem (i.e., xylem area exposed to pathogens with a loss of its normal functions), wound xylem (i.e., mass of lignified and well-differentiated cells overgrowing the wound from its margins) and callus mark (i.e., a layer of undifferentiated cells which are characterized by numerous vacuoles and high metabolic activity that may assist recovery of the vascular cambium from the wound edges). At the microscopic level, the main strategy of a tree to respond to mechanical wounding is through the preferred formation of hydraulically more efficient cells (Zimmermann 1983), which ensures moisture maintenance next to wounds and thus limits fungal infection (Boddy and Rayner 1983) and/or vascular system collapse.

A large body of studies has described the impacts of scarring on the wood anatomy of broadleaved trees (Rier and Shigo 1972; Rademacher et al. 1984; Lev-Yadun and Aloni 1993; Stobbe et al. 2002; Schweingruber 2007; Arbellay et al. 2010; Ballesteros et al. 2010a, b; Kames et al. 2011). Arbellay et al. (2012a) and Ballesteros et al. (2010a, b) observed the generation of smaller and isometric cells as well as stronger radial structures (i.e., rays) after wounding, causing relative changes in wood density (i.e., Hacke et al. 2001). Specifically, young *Fraxinus excelsior* L. trees wounded by floods have been found to produce much smaller vessel lumina and a significantly larger number of rays in the 30° sector next to the wound (Arbellay et al. 2012a). In *Betula pubescens* Ehrh., wounds induced by snow avalanches have been shown to induce a significant reduction of earlywood vessel lumina in the 2 years following cambial injury (Arbellay et al. (2012b). Similar patterns have also been observed in *Alnus incana* (L.) Moench. injured by snow avalanches (Arbellay et al. 2012b) and *Alnus glutinosa* L., *Fraxinus angustifolia* Vahl., and *Quercus pyrenaica* Willd. injured by torrential floods in Mediterranean ecosystems (Ballesteros et al. 2010b). All of the above changes in wood anatomy have been interpreted as a requirement of trees to improve xylem hydraulic safety and mechanical strength (Arbellay et al. 2012a, 2014a, b) and were shown to cause a local impact on wood density (Fonti et al. 2012).

Beyond the physiological consequences to the tree, wounds also represent an excellent means to date those processes that influenced the development of the tree during its lifetime (Stoffel et al. 2010; Stoffel 2008; Stoffel and Corona 2014). Through the identification and tree-ring dating of anatomical changes next to wounds, researchers have been able to reconstruct past hydrogeomorphic activity such as floods (Ballesteros et al. 2010a, b; 2011a, b), debris flows (Bollschweiler et al. 2008; Bollschweiler and Stoffel 2010), snow avalanches (Stoffel and Hitz 2008; Stoffel et al. 2013), rockfalls (Schneuwly et al. 2009a; Trappmann et al. 2013) or fires (Arbellay et al. 2014a, b), among others. However, efficient wound dating on living trees is subject to detailed knowledge of the area affected in the three dimensions of the stem (Schneuwly et al. 2009b; Arbellay et al. 2012a; Kogelnig-Mayer et al. 2013). Therefore, it is recognized that more efforts are still needed to better understand changes induced to trees after wounding, and even more so in broadleaved trees (Stoffel and Corona 2014). In this context, the analysis of X-ray computed tomography (XRCT) derived images allows visual detection of internal wood structures and represents an excellent tool for a visual 3D characterization of internal features related to wounds (Bill et al. 2012; Stoffel and Klinkmüller 2013; Guardiola-Albert et al. 2015). In addition, the information recorded by pixel values of XRCT images is related with wood density (Leban et al. 2004) and can thus be studied quantitatively using geostatistical approaches. Therefore, tonal variations in the spatial domain can be described in terms of the two main conceptual components associated to pixels units, variability and spatial correlation. The geostatistical approach assumes that pixel values are spatially distributed following a structure, which is given by the spatial correlation. Variability and spatial correlation are therefore modeled jointly with the variogram function, which expresses semi-variance as a function of distance, and possibly direction (Guardiola-Albert et al. 2015).

In this study, we present a novel methodology based on the combined analysis of XRCT images and geostatistical functions to detect and quantify macroscopic features and the extension of wood changes after wounding of three riparian species by floods (i.e., *Alnus glutinosa* (L.) Gaertn., *Fraxinus angustifolia* Vhal. and *Salix atrocinerea* Brot.). In particular, this paper aims at (1) defining the tangential influence of wounds on riparian trees, and at (2) studying controls of different tree and wound characteristics on the extension of wounds and associated tissues. Results are expected to improve our understanding of the 3D response of riparian trees to wounding.

Materials and methods

Sampling and XRCT image acquisition

In summer 2011, we sampled 30 mature riparian trees (12 *A. glutinosa*, 10 *F. angustifolia*, and 8 *S. atrocinerea*) damaged by floods in the Alberche river (Spanish Central System; 40°23′50″N; 4°50′50″W; 860 m a.s.l.). Large enough stem sections were selected to obtain the full portion of the stem affected by wounding and stored in a cool and humid place to avoid the formation of drying cracks and to maintain wood humidity so as to improve the quality of XRCT imagers. Mean sample length was 67 cm (±45 cm; max: 243 cm; min: 19 cm) with a mean diameter of 12 cm (±5 cm; max: 26 cm; min: 5 cm).

3D images from all wounded stems were acquired at the Institute of Forensic Medicine, University of Bern, with a slice thickness of 1.25 mm using a Siemens Emotion 6 XRCT operated at 130 kV and 88,200 mA beam current. More than 30,000 images (>30 Gb) were quantized during this process in 16-bit grayscale and stored in DICOM (Digital Imaging and Communication in Medicine) format. The pixel gray level of XRCT imagers represents the X-ray attenuation coefficient, which is proportional to the amount of X-ray energy absorbed and consequently the relative density of the analyzed material (Longuetaud et al. 2005). The resulting images or slices had a size of 512 × 512 pixels, with a variable pixel size close to 0.3 mm.

Analyzing macroscopic wood characteristic-related wounds

Macroscopic features induced by flood damage to cambial tissue as well as growth patterns next and opposite to wounds were then studied on 8–10 slices per wound. Slices were selected according to their longitudinal position with respect to the scar so as to characterize longitudinal changes in wound characteristics as well as to capture phenomena at wound edges. Analysis included (1) the nature of the wound (i.e., open/closed scar; called STATE), (2) tree age (AGE), (3) wound date (EVENT), (4) tree diameter (DIAM), (5) wound radii (WR), (6) wound length (WL), (7) wound width (WS), (8) observed decayed area (DECAY), as well as (9) length of the overgrowing pad involved in wound closure (CR) and (10) length of the callus mark at the edge of the wound (CM). In addition, we recorded the growth pattern of the trees, in particular for the years prior to and after wounding (Fig. 1).

Samples were then divided into two categories according to their capacity to recover from wounding and the existence of previous wounds. We consider trees to belong to health state I (HS I) if they lack any sign of suppressed growth after wounding and if they have not any previous (internal) scar. Health state II (HS II) trees, instead, exhibit moderate to strong growth suppression and limited recovery after wounding (Stoffel and Corona 2014) and/or already were injured in the past (multiple internal scars).

Visualization of XRCT images and the quantitative analysis of macroscopic features were performed with the public domain software ImageJ (Abràmoff et al. 2004). All samples were initially imported as image sequences and the 3D viewer package was used to visualize XRCT images in 3D. Different filters and color ramps were applied in post-processing so as to increase contrast and to accentuate details in images or in the selection (Fig. 2).

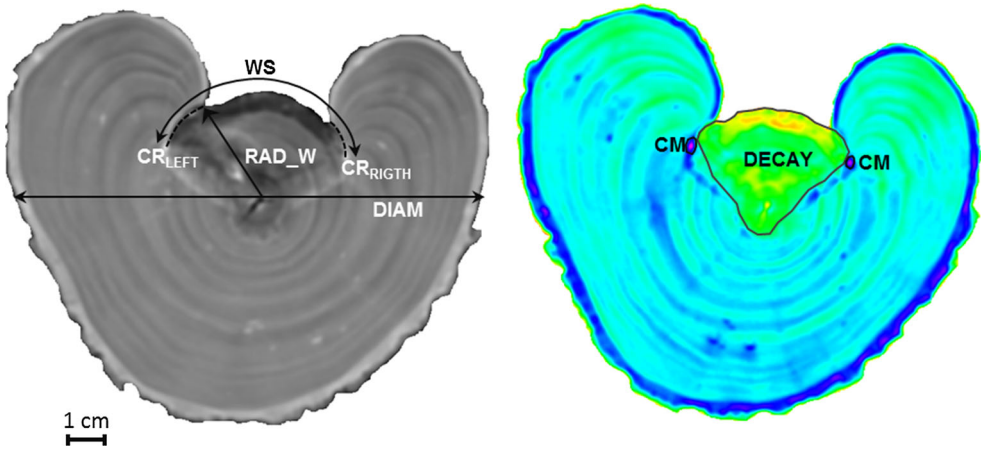

Fig. 1 Definition of parameters measured on XRCT slices: (*left*) DIAM represents the diameter of the tree measured perpendicular to the damage, RAD_W indicates the radius at the moment of impact, WS represents the length of damaged cambial tissue, and CR_{LEFT} and CR_{RIGHT} are the lengths of the callus; (*right*) DECAY represents the area affected by decay processes and CM shows the callus mark at both sides of the wound, formed by rounded meristematic cells. Anatomical changes are noted through the existing *color* change in the callus pad

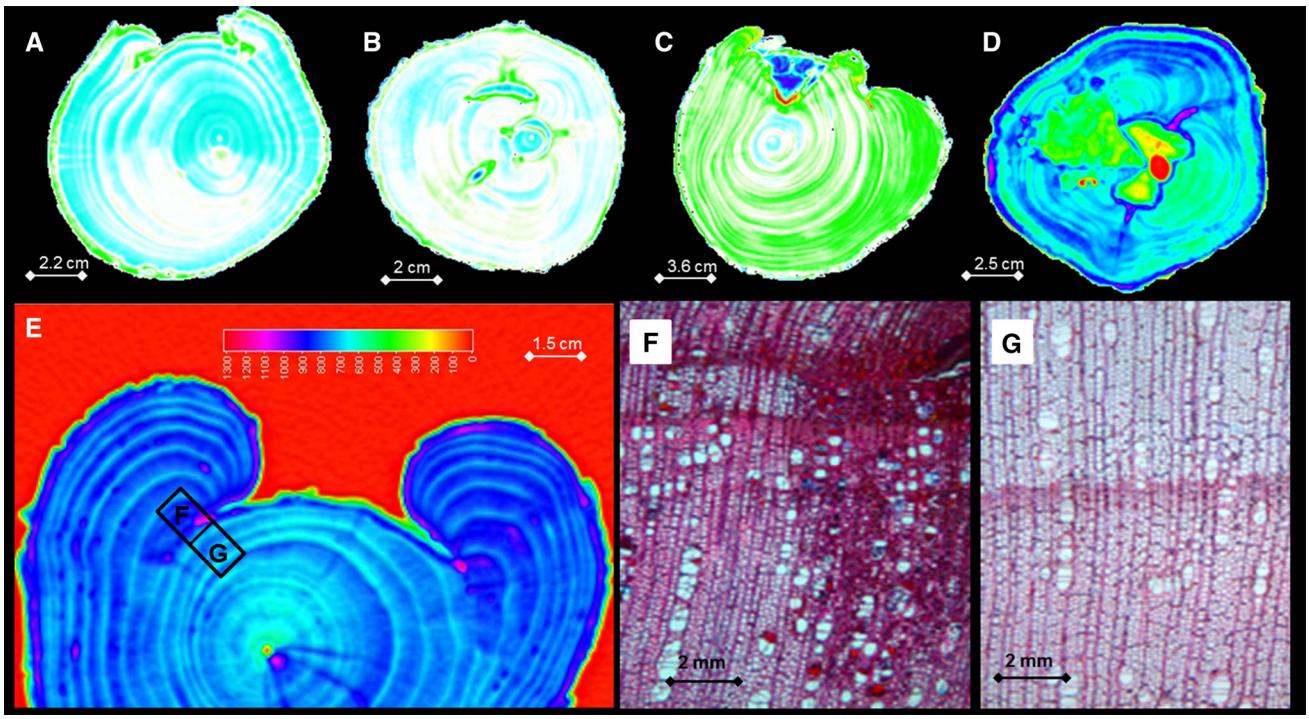

Fig. 2 Cross-sectional XRCT view of different riparian broadleaved trees affected by floods: **a** Healthy broadleaved tree with absence of internal scars and recovery of growth rates after wounding; **b**, **c**, **d** examples of riparian trees with bad health as a consequence of multiple scars and the absence of post-wounding growth recovery. **c**, **d** Reaction area is clearly observed in the border of the wounded xylem and around the wound (on *green*, **a** and **b**) as well as insolating the decay area in **c**. The *blueish* and *greenish-yellowish colors* point to different states of decay; **e** represents a cross-sectional view after filter processing to highlight the callus mark (CM, in *purple*) (**f**, **g**) Micro-cuts with wound-related anatomical features

Analyzing wood change properties using the variogram function

A 1D variogram function was used to identify and quantify changes in wood properties. Variograms are a quantitative descriptive statistical tool used for the characterization of the spatial continuity of a dataset such as pixel values (Cressie 1992). The variogram function represents the variance of the difference between field values at two locations (Cressie 1992). It is represented by a sill (i.e., an ordinate value where the variogram levels off), a range (i.e., distance at which this leveling off occurs) and a nugget (i.e., semi-variance at the origin). We used raw pixel data from XRCT slices at different radii (pith to bark) to quantify the tangential anisotropy in pixel values stemming from cambial wounding. Raw data from pixels in each radial direction were obtained with the software ImageJ using the plot profile tool. Radial directions from pith to bark were defined with tangential steps of 5° from the wound edges and up to 180°, and at every 20° interval in the remaining segments (Fig. 3). 1D variograms were computed by means of the following equation (Eq. 1).

$$\gamma(h) = \frac{1}{2N}\sum_{i=1}^{N}[z(x_i) - z(x_i + h)]^2 \quad (1)$$

where Υ(h) represents the computed variogram; N is the number of data sample pairs separated at a distance h; $z(x_i)$ are gray-level sample values; and $z(x_i + h)$ are all the gray-level sample values at a distance h from point x_i. In experimental variograms, one assumes that the higher the sill the higher the pixel value variance, and consequently also the higher the density variance. Because higher wood densities will result in higher gray-level pixel values in the XRCT images, samples with bigger sills (i.e., higher pixel values) can be related to denser wood (Freyburger et al. 2009; Guardiola-Albert et al. 2015). Consequently, discrepancies in variogram sills at small distances are therefore assumed to represent tree reactions to impacts (Guardiola-Albert et al. 2015).

Statistical procedures

Two different statistical procedures have been applied to the data to interpret results. We first carried out a descriptive statistical analysis of macroscopic feature

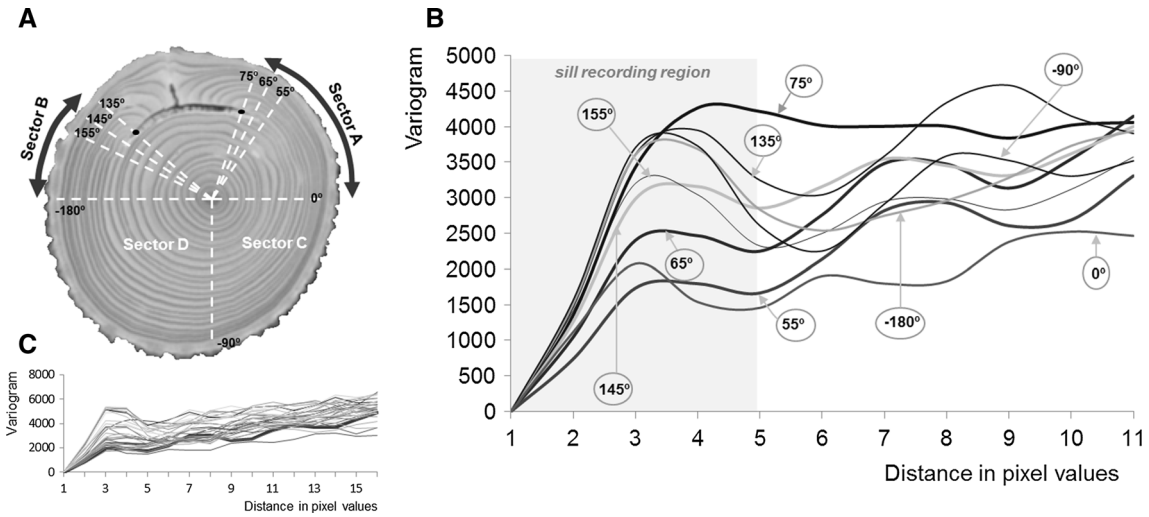

Fig. 3 **a** Schematic view of the criteria used to compute 1D variograms. In sectors *A* and *B*, located closer to the wound, variograms were computed for every 5°. In sectors *C* and *D*, tangential distances between measurements were chosen between 10 and 45° so as to avoid noisy signals induced through the presence of reaction wood; **b** Higher sill values are associated with high-density wood and typically located close to wound edges; **c** Example of a hole-type variogram computed for the cross-section represented in **a**

observations to organize and evaluate the nature of data. To detect the maximum tangential affected angle (TAA) by wounding, we performed non-parametric Wilcoxon tests at 95 % least significant difference (LSD) and focused on the identification of tangential angles for which differences between sill values of different radial directions were statistically significant. During this step, we also eliminated samples with zones of advanced decay to avoid misinterpretation. Therefore, our results refer to changes in xylem from the wound edges. Finally, we also performed a principal component analysis (PCA) and matrix correlations to analyze the relation between anatomical feature observation and TAA for each sample.

Results

Macroscopic anatomical features description of wounds induced by floods

Table 1 and Fig. 4 show the characterization of macroscopic features of wounds using a total of 444 images from 12 *A. glutinosa*, 10 *F. angustifolia* and 8 *S. atrocinerea* stem sections. More than two-thirds of the samples (>70 %) show signs of advanced decay and have thus been considered to belong to HS II. Decay is most present in samples with severe or multiple wounding. Mean tree age was homogeneous between the species and ca. 17 years,

Table 1 Macroscopic anatomical features of trees used for XRCF analyses

	Alnus glutinosa		*Fraxinus angustifolia*		*Salix atrocinerea*	
	I	II	I	II	I	II
TREE (n of slices)	4 (40)	8 (80)	2 (20)	8	2	6
AGE (in years)	17.8 ± 6.1	16.8 ± 4.3	23.5 ± 1	17.1 ± 7.8	17	18.8 ± 9.3
DIAM (mm)	144.6 ± 78.3	121.4 ± 36	89.9 ± 11.5	96.4 ± 37.0	86.2 ± 10.2	114.6 ± 24.2
No. injuries (o/c)	7 (4/3)	14 (11/3)	2 (2/0)	11 (10/1)	2 (2/0)	12 (10/2)
RAD_W (mm)	26.2 ± 18.8	37.3 ± 14.3	22.3 ± 6.46	36.9 ± 20.4	24.4 ± 2.9	21.6 ± 11.2
WS (mm)	40.28 ± 48.6	28.6 ± 31.6	11.7 ± 8.01	20.3 ± 18.8	7.7 ± 6.3	9.7 ± 9.7
WL (mm)	248.24 ± 140.2	298.1 ± 271.2	93.1 ± 29.5	175.9 ± 209.3	151.2 ± 107.7	185.0 ± 153.7
RWD (%)	24.5 ± 18.3	14.1 ± 14.8	8.5 ± 4.7	9.7 ± 8.8	4.8 ± 3.5	12.1 ± 15.6
CR (mm)	16.3 ± 18.7	8.2 ± 6.3	3.9 ± 1.8	10.6 ± 9.6	2.8 ± 0.6	4.8 ± 4.5
DECAY (mm^2)	368.9 ± 429.2	248.9 ± 395.7	28.4 ± 13.9	64.1 ± 61.4	299.5 ± 107.9	204.9 ± 321.8
CM (mm)	5.9 ± 4.8	4.7 ± 2.8	2.8 ± 1.9	2.9 ± 2.6	1.18 ± 0.20	3.8 ± 3.6

No. injuries (o/c) indicate number of injuries open (o) and closed (c), whereas RWD indicate percentage of cambium tissues damages. Remaining parameters are defined in the text

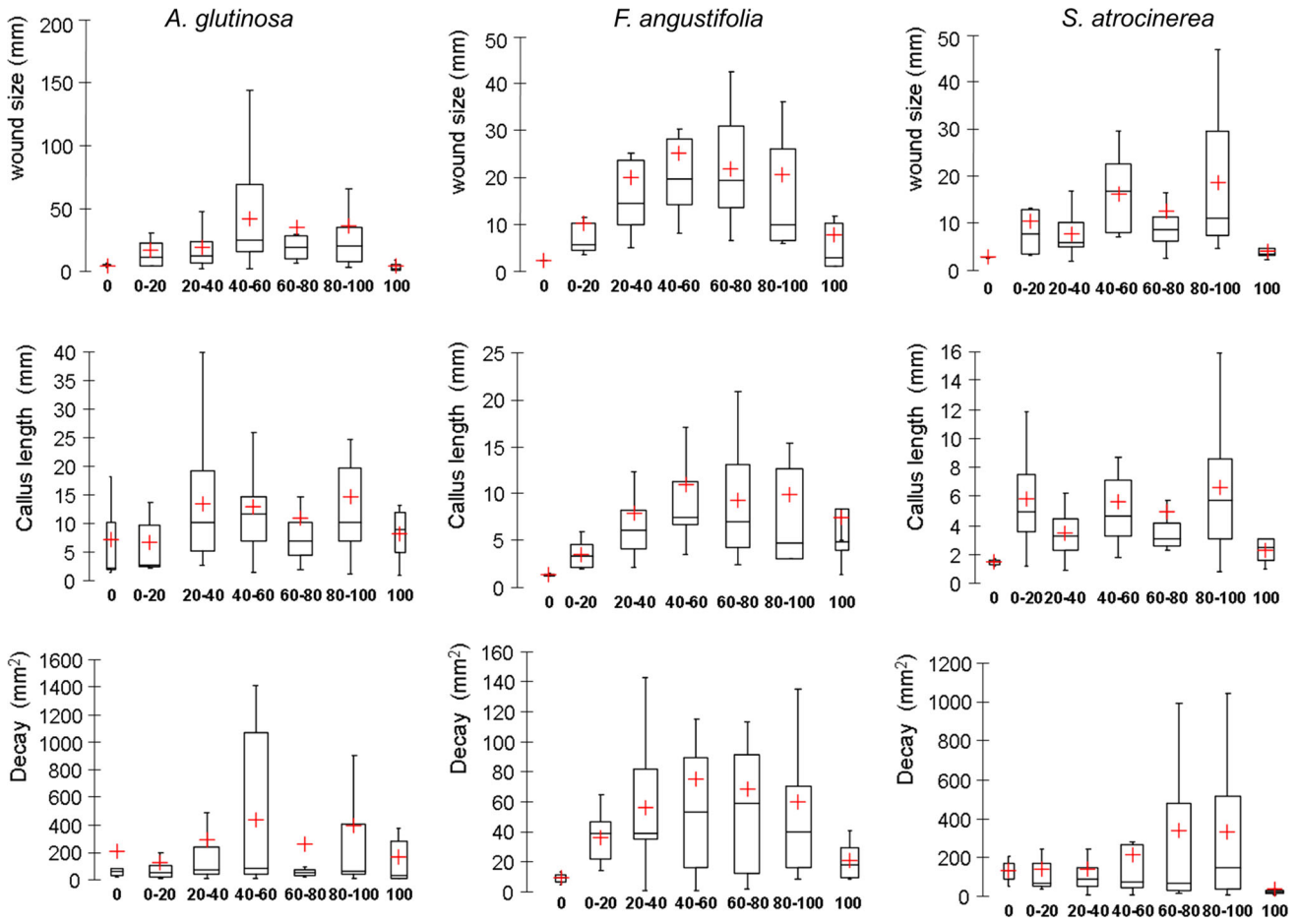

Fig. 4 Differences in wound size, callus length and decay area along the vertical distribution of the scar. The x-axis represents the relative length of the wound slice in percentage (%)

with the exception of HS I *F. angustifolia* for which trees had an average age of 23 years. The sample used in this study thus consists of trees which are in the transition between the juvenile and mature stages. Forty-eight flood wounds—with almost 80 % of them in the form of open wounds—were dated to 13 different flood years between 1989 and 2009, with more replications in more recent years (i.e., 9 wounds inflicted by a flood in 2004 and 7 wounds attributed to floods in 2006 and 2001, respectively).

Wound radii are comparable between species and range from 21.6 to 37.3 mm, but *A. glutinosa* presented a larger percentage of cambial tissue damage as compared to *S. atrocinerea* or *F. angustifolia* (up to 24.5, 12.1, and 9.7 %, respectively). Wound shape was generally oval and with larger widths in the central portion of the injury (Fig. 4). The ratio defined between WS and WL (which ranged from 0.16 to 0.4) suggests that injuries were elongated, presumably reflecting the axial direction of wood fibers. Larger wound sizes are observed in HS II samples of *F. angustifolia* and *S. atrocinerea*, whereas injuries were larger in *A. glutinosa* if they belonged to HS I. *A. glutinosa* also presented more samples with multiple wounds (up to 75 % of all samples) than *S. atrocinerea* and *F. angustifolia* where multiple scars were virtually absent with 0.5 and 0.1 % of all cases, respectively.

Visual inspection also allowed adequate distinction between the size and state of decay processes. Averaged measurements of decay area indicate that diffuse-porous *A. glutinosa* and *S. atrocinerea* present significantly larger decay areas (between 204.9 ± 321.8 and 368.9 ± 429.2 mm^2) than ring-porous *F. angustifolia*, where decay only affected between 28.4 ± 13.9 and 64.1 ± 61.1 mm^2. In addition, decay was generally more important in the central portions than at the upper and lower 20 % of the wound (Fig. 4).

A. glutinosa presented longer overgrowing pads (between 8.2 and 16.3 mm) than *F. angustifolia* and *S. atrocinerea*, where overgrowing pads ranged between 3.6–10.6 and 2.8–4.8 mm, respectively. This observation seems to indicate that *A. glutinosa* may have higher closure rates on average than the other two species. In addition, callus marks at the wound edges were larger in *A. glutinosa*

(4.7–5.9 mm) than in *S. atrocinerea* (1.1–3.8 mm) and *F. angustifolia* (~2.8 mm).

Tangential extension of the affection induced by wounds

Twenty-three samples (62 %) were used for variogram analysis (7 *A. glutinosa,* 9 *F. angustifolia*, and 7 *S. atrocinerea*). The 1D variogram analysis reported significantly ($p < 0.05$) higher sill values near the wound edges as compared to reference slices taken from undamaged stem cross-sections (Fig. 5a). The averaged TAA varied between 10° and 20° with a deviation between 2° and 16.6°. Trees belonging to HS I presented generally lower TAA than those belonging to HS II. The highest TAA values were found in *A. glutinosa* with averaged TAA values of 17.7 ± 9.3° ($n = 29$) and 20 ± 16.6° ($n = 20$) for health states I and II, respectively. In *F. angustifolia,* TAA values ranged from 10.8 ± 2° ($n = 10$) to 15.9 ± 14.3° ($n = 47$), whereas maximum TAA values in *S. atrocinerea* were 10 ± 8.6° ($n = 11$) and 12.8 ± 6.5° ($n = 32$). In longitudinal direction, TAA values were highest in the central parts of the wounds (Fig. 5b). Observations are not significantly correlated ($r^2 \sim 0.2$) but the observed trend is certainly characterized by higher values at slice depths comprised between 30 and 90 % .

Controls on TAA and DECAY variables

Figure 6 indicates that the relationship between wound characteristics and TAA depends quite clearly on species and health state. In addition, Table 2 shows correlation values between macroscopic features and TAA quantified for each species and for both health states.

Figure 6 also illustrates that two factors explain 74.9 % of the variability in HS I *A. glutinosa* ($n = 24$). The first factor explaining 55.8 % of the variability is a combination of all variables with the exception of TREE and EVENT. TAA is weakly correlated with wound size (WS = 0.40) in these samples, whereas DECAY was related with wound size parameters (RW = 0.6; WS = 0.74) and wound closure rate (CR = 0.65). Correlation also exists between DECAY and TREE (0.66), showing the dependence of individual DECAY processes. However, negative correlations are observed with time passed since wounding (EVENT = −0.65), indicating that younger trees (which are presumably also smaller) exhibit smaller areas affected by decay (DECAY). In HS II *A. glutinosa* trees ($n = 19$), variability can be explained in 59.6 % using only two factors. Here, the first factor is related to TAA and CM (positive correlations: 0.72) and the second to WS and RW. In this case, we also observe weak negative correlations between TAA and TREE (−0.46) and CR (−0.49). We do not, however, observe clear correlations between DECAY and any of the remaining variables.

In HS I *F. angustifolia* trees ($n = 10$), the two first factors explain 90.3 % of the variability, whereas only 55.6 % of the variability can be explained in the samples with HS II ($n = 46$). In the first case, TAA was clearly controlled by the tree and wound size variables WS (0.78), RW (0.96), and CR (0.93). The first factor therefore explained most of the variability (79.7 %) and was related with all variables with the exception of EVENT and CM. DECAY area was related with wound size (RW = 0.96 and WS = 0.78), indicating that the decay process is clearly conditioned by the size of the wound and the size of the tree at the time of wounding. Furthermore, DECAY area was also positively correlated with CR (0.73) and individual trees (0.88), and negatively correlated with EVENT (−0.88). By contrast, we could not see any control on TAA values of HS II *F. angustifolia* samples, and only DECAY showed a correlation with EVENT (0.72).

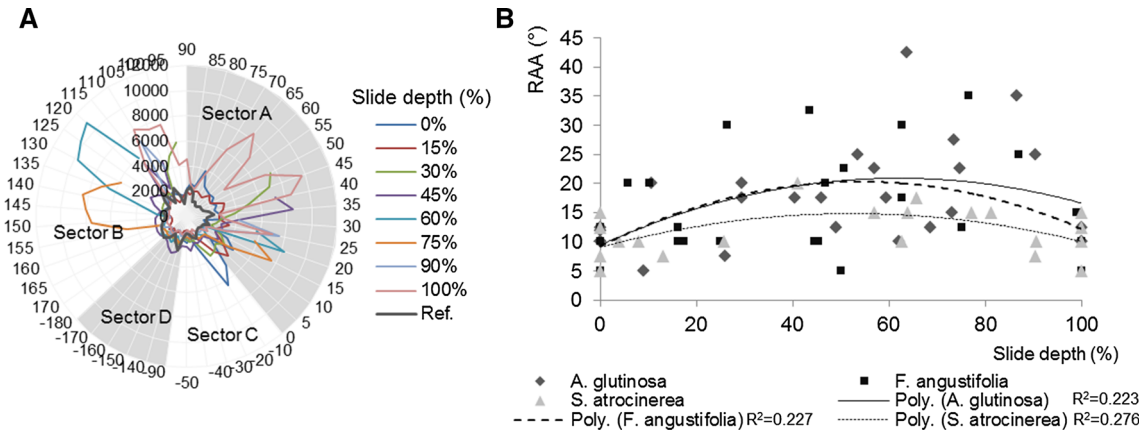

Fig. 5 **a** Radial plot of maximum sill values recorded with a variogram with slices taken at different locations along the scar; **b** the maximum TAA is located in the central part of the scar, between 40 and 80 % of the scar length

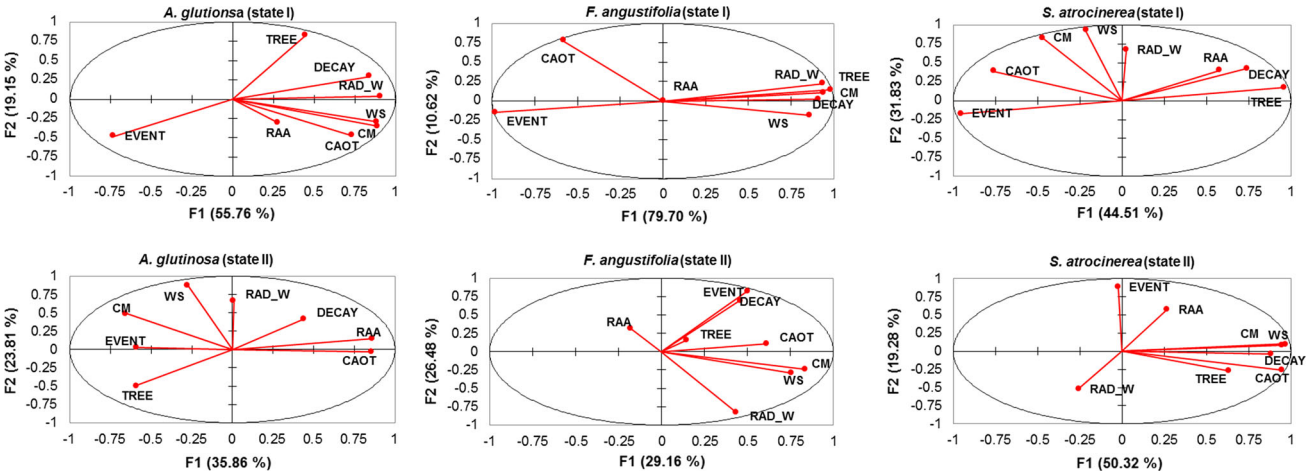

Fig. 6 Results of the principal component analysis (PCA) for *A. glutinosa*, *F. angustifolia*, and *S. atrocinerea* and for HS I and II (for details see text)

Table 2 Matrix correlations (Pearson's n) as suggested by the principal component analysis (PCA)

	TAA	DECAY	TREE	EVENT	RAD_W	WS	CR	CM
A. glutinosa								
TAA	1.00	*0.55*	*−0.46*	*−0.25*	*0.00*	*−0.06*	*−0.49*	*0.72*
DECAY	0.34	1.00	*−0.30*	*−0.07*	*−0.12*	*0.15*	*0.23*	*0.38*
TREE	−0.05	0.66	1.00	*0.30*	*−0.38*	*−0.17*	*0.27*	*−0.31*
EVENT	−0.10	−0.65	−0.60	1.00	*−0.03*	*0.07*	*0.37*	*−0.49*
RAD_W	0.03	0.60	0.37	−0.79	1.00	*0.53*	*0.01*	*−0.02*
WS	0.40	0.74	0.21	−0.35	0.73	1.00	*0.60*	*−0.24*
CR	0.22	0.65	0.07	−0.45	0.80	0.98	1.00	*0.42*
CM	0.25	0.37	−0.03	−0.36	0.71	0.70	0.71	1.00
F. angustifolia								
TAA	1.00	*−0.08*	*−0.30*	*0.18*	*−0.39*	*−0.05*	*0.04*	*−0.13*
DECAY	0.88	1.00	*0.19*	*0.72*	*−0.28*	*0.13*	*0.11*	*0.24*
TREE	1.00	0.88	1.00	*0.23*	*0.14*	*0.02*	*−0.25*	*0.12*
EVENT	−1.00	−0.88	−1.00	1.00	*−0.48*	*0.13*	*0.30*	*0.32*
RAD_W	0.96	0.77	0.96	−0.96	1.00	*0.44*	*0.49*	*0.19*
WS	0.78	0.89	0.78	−0.78	0.63	1.00	*0.70*	*0.16*
CR	0.93	0.73	0.93	−0.93	0.96	0.72	1.00	*0.36*
CM	−0.48	−0.45	−0.48	0.48	−0.43	−0.54	−0.51	1.00
S. atrocinerea								
TAA	1.00	*0.29*	*0.15*	*0.38*	*−0.01*	*0.17*	*0.24*	*0.07*
DECAY	0.25	1.00	*0.39*	*−0.04*	*−0.01*	*0.83*	*0.83*	*0.80*
TREE	0.47	0.91	1.00	*−0.11*	*0.08*	*0.45*	*0.50*	*0.66*
EVENT	−0.47	−0.91	−1.00	1.00	*−0.28*	*0.06*	*0.07*	*−0.29*
RAD_W	0.76	−0.07	−0.01	0.01	1.00	*−0.32*	*−0.31*	*−0.24*
WS	0.14	0.26	−0.03	0.03	0.51	1.00	*0.95*	*0.84*
CR	−0.13	0.14	−0.25	0.25	0.32	0.93	1.00	*0.88*
CM	−0.44	−0.18	−0.59	0.59	0.05	0.45	0.74	1.00

Values in italics belong to trees of HS II

Observed variability in *S. atrocinerea* was explained by almost 76.3 and 69.6 % for HS I ($n = 11$) and HS II ($n = 28$). For HS I samples, a clear difference can be observed between factors. The first factor is explained by response variables (TAA, DECAY) and TREES, whereas the second factor is explained by wound and tree size

variables (WS, RW). Main correlation was observed between TAA and RW (0.76) for HS I samples, and additional correlations exist between DECAY and WS (0.83), as well as with CR (0.83) and CM (0.80). Again, only negative correlations exist between DECAY and EVENT (−0.91) and a high dependence between DECAY and individual trees (TREE = 0.91) for samples belonging to HS II.

Discussion

Wounding in broadleaved trees has been reported to induce changes in wood structures through the formation of narrower vessels, flattened and smaller fibers, and different parenchyma cells, thus resulting in increased relative xylem density (Lev-Yadun and Aloni 1993; Arbellay et al. 2010; Ballesteros et al. 2010a, b; Aloni and Zimmermann 1984; Kuroda 1986; Hacke et al. 2001). In addition, callus tissue, formed immediately after wounding at the wound margins, is characterized by fewer vessels, but the number of vessel structures has also been shown to increase again in the years following wounding (Stobbe et al. 2002; Ballesteros et al. 2010b; Arbellay et al. 2012a, b). These anatomical modifications, which are linked to changes in radial structures (Arbellay et al. 2012a), induce a change in wood density (Hacke et al. 2001). In this study, we have contrasted findings from anatomical analyses after wounding with information contained in XRCT images. Similar to Longuetaud et al. (2005), Fromm et al. (2001) or Meincken and Plessis (2013), we used X-ray computed tomography to acquire images of internal wood structures and to detect relative changes in wood density. In contrast to previous work, we included geostatistical approaches to quantify wound-related wood changes and to determine their tangential extension along the stem. Results indicate average tangential extensions of wounds and related wood densities ranging between 17.7 and 20.0° in *A. glutinosa*, 10.8° and 15.9° in *F. angustifolia*, and 10° and 12.8° in *S. atrocinerea*. Our findings are in line with Arbellay et al. (2012a) who identified wound-induced anatomical changes at tangential distances of up to 25° from the wound edges, but with more obvious (or significant) changes being limited to the first 15°.

The fact that XRCT data match quite well with results from microscopic studies reinforces the validity of variogram approaches for the description of spatial patterns of images (Jupp et al. 1988) with varying results (Atkinson and Lewis 2000). This contribution also confirms the potential of systematic geostatistical techniques (Guardiola-Albert et al. 2015) to determine changes in wood properties, and demonstrates clearly that variograms represent an appropriate tool to describe the spatial variability of pixel values in XRCT images, and hence changes in wood density.

However, some issues related to the use of variograms in XRCT-based wood image analysis remain and need to be addressed in future research. During analysis, we observed cyclicity in computed variograms which can be explained by the nature of xylem. We realize that 1D whole variograms are most appropriate for research purposes as they typically exhibit sinusoidal waves which form peaks and troughs (Journel and Huijbregts 1978; Ma and Jones 2001), thereby conveying the cyclicity of the underlying phenomenon (i.e., tree rings). As cyclicity was absent very close to the wound, it could thus be used to delineate the area affected by wounding. We also confirm that tree rings clearly prevent the use of multi-dimensional variograms (Guardiola-Albert et al. 2015). In addition, attempts to perform variograms along the tangential direction of tree rings clearly failed in the case of narrow rings close to wounds. Other issues such as internal variations in moisture content stemming from physiological factors as well as reaction wood or solvent extractives may influence the observed anisotropy derived from density variations as well (Bucur 2003). In this regard, a careful selection of slices with homogenous xylem tissue or the previous use of extraction procedures (i.e., Soxhlet extractor) could minimize such effects during variogram analyses.

The response of mature riparian trees to flood damage varied substantially between species, despite the fact that all trees were growing in the same environment. Changes in wood density and related anatomical features were more evident in *A. glutinosa* than in *S. atrocienera* and *F. angustifolia*, and thus support the theoretical concept of differences in genetic drivers of wound healing between species (Deflorio et al. 2008; Dujesiefken et al. 2005; Lowerts and Kellison 1981; Reymond et al. 2000). In addition, differing bark and xylem structures also seem to determine tree as well as decay processes. Much larger wounds and larger decay areas were observed in diffuse-porous *A. glutinosa* and *S. atrocinerea* than in ring-porous *F. angustifolia*. These differences can possibly be attributed to differences in hydraulic efficiency between the two xylem structures and are presumably favored by softer bark tissues in *A. glutinosa* and *S. atrocinerea* (Lowerts and Kellison 1981; Ballesteros et al. 2010a; Trappmann and Stoffel 2012). The larger number of vessels in diffuse-porous species could at the same time, however, also ease the infection of trees by pathogens (Schwarze and Baum 2000).

At the level of individual trees, we observe a strong influence of the health state and/or presence of older wounds on the capacity of a tree to respond to damage, which is in line with previous findings by (Pearce et al. 1997; Pearce 2000). In trees with HS I, responses were

more commensurate with tree and wound size variables, whereas in trees with HS II, correlations between variables were almost completely missing. Our results clearly support the findings of Arbellay et al. (2012a) who underlined that the strength and persistence of wound-induced anatomical anomalies would depend above all on tree species, but also on tree vigor and wound size. We therefore confirm that the inclusion of the history and traits of individual trees is relevant for the understanding of mechanisms driving tree response to damage (Romero et al. 2009).

We also observe a dependency of callus pad length and callus mark size on species and health state, and thereby confirm findings from previous work (Kozlowski 1971; Neely 1988; Haavik and Stephen 2011; Schneuwly-Bollschweiler and Schneuwly 2012). Observations also confirm that *A. glutinosa*, good pre-wounding health conditions provided, exhibits higher callus recovery rates and greater chaotic marks than the other species analyzed, and that the species therefore seems to be highly adapted to riparian environments where damage caused by hydrological events may occur repeatedly. As soon as the health state worsens, however, callus recovery will decrease drastically in *A. glutinosa* as well and by almost 50 %.

The tangential affected area by wounding will favor a sudden loss of moisture content and more aeration in the damaged tissue, and thus facilitate the colonization and development of pathogens competing for available nutrients; thereby degrading living cells and initiating the process of decay (Boddy and Rayner 1983; Baum and Schwarze 2002). Changes in moisture content and aeration will be limited by compartmentalization of wound-induced structures (Boddy and Rayner 1983), whereby large wounds will typically be at high risk to embolism. Differentiation of smaller and denser structures, as confirmed to occur in our samples after wounding, can thus be regarded as (1) an adaptive trade-off between xylem safety and hydraulic efficiency, (2) a way to avoid embolism (Hacke et al. 2006), and as (3) a strategy to maintain water content in cells (or even favor an increase in water content in healthy wood (Pearce et al. 1997), thereby (4) preventing inactivity of parenchyma cells which would again result in favorable conditions for the growth of wood-decay pathogens (Boddy and Rayner 1983; Pearce 2000; Rayner 1986; Boddy 1992).

In addition, it seems likely that differences in the availability of energy (i.e., carbohydrates) stored in the xylem radial system (rays) can be used to explain differences in variables observed in our tree samples of different health state (Shigo 1984). In *A. glutinosa* and *F. angustifolia*, decay processes in trees with good initial health conditions were above all related to wound and tree size at the time of scarring, whereas such correlations were clearly absent in trees with poor health state. In the latter case, previous wounding is thought to have generated a decline in energy reserves and metabolizing capacity as a consequence of decreased water-transport efficiency. Moisture decrease in previously affected internal tissue will also facilitate access to pioneering microorganisms which in turn will oxidize and polymerize phenolic compounds. Here, tree response to wounding may be controlled by external and random environmental factors related to the succession of microorganisms affecting the newly exposed sapwood (Lowerts and Kellison 1981). In *S. atrocinerea*, by contrast, correlation between decay and other variables showed a completely different behavior. Trees with good pre-wounding health conditions did not reveal noteworthy correlations, whereas in trees with poor health conditions, decay, wound size and/or tree diameter control the tangential extension of the affected area. We interpret this finding as being the result of an increased risk of infection in the central part of the wounded area as compared to the more distal and smaller areas.

Conclusions

The combination of geostatistics (i.e., variogram function) and X-ray computed tomography (XRCT) images is a valuable approach for the quantification of 3D structural changes in riparian trees affected by floods. *A. glutinosa* has been demonstrated to suffer most from flood damage and presented larger tangential extensions and areas affected by decay after scarring than *S. atrocinerea* and *F. angustifolia*, but the intensity and characteristics of tree response has also been shown to depend clearly on the health state of trees prior to wounding. In healthy trees, reactions to wounding are driven clearly by wound size, whereas the response will be controlled by external factors related to the dynamics of pathogens and loss of vitality (i.e., tree energy) in the trees with the poorest health. This study has also demonstrated the potential of XRCT in recording relative changes in wood properties (i.e., wood density) after wounding, and thus provides a methodological basis for future work. Therefore, we conclude that the use of geostatistical image analysis may improve our understanding of intrinsic and external (e.g., climatic) factors on cambial activity in general and wood density in particular and, in combination with other techniques, to help the theoretical modeling of cambial tissue under different scenarios.

Author contribution statement JABC MS CG: conceived and designed the experiments. JAB MS CG: performed the experiments. JABC: analyzed the data. JABC MS CG: contributed reagents/materials/analysis tools. JABC MS CG: wrote the paper.

Acknowledgments The authors are grateful to the Forensic Institute of the University of Bern for access to the XRCT device, and to the Tragsa Avila foresters for field support. This study has been partially funded by the project CGL2010-19274 (projects MAS Dendro-Avenidas) of the Spanish Ministry of Economy and Competitiveness. Kevin T. Smith, Estelle Arbellay and two anonymous reviewers provided valuable and detailed feedback on an earlier version of this manuscript.

Conflict of interest The authors declare that they have no conflict of interest.

References

Abràmoff M, Magalhães P, Ram S (2004) Image processing with imagej. Biophotonics Int 11(7):36–42

Aloni R, Zimmermann MH (1984) Length, width and pattern of regenerative vessels along strips of vascular tissue. Bot Gaz 145:50–54

Arbellay E, Stoffel M, Bollschweiler M (2010) Wood anatomical analysis of *Alnus incana* and *Betula pendula* injured by a debris-flow event. Tree Physiol 30:1290–1298

Arbellay E, Corona C, Stoffel M, Fonti P, Decaulne A (2012a) Defining an adequate sample of earlywood vessels for retrospective injury detection in diffuse-porous species. PLoS One 7:e38824

Arbellay E, Fonti P, Stoffel M (2012b) Duration and extension of anatomical changes in wood structure after cambial injury. J Exp Bot 63:3271–3277

Arbellay E, Stoffel M, Sutherland EK, Smith KT, Falk DA (2014a) Changes in tracheid and ray traits in fire scars of North American conifers and their ecophysiological implications. Ann Bot 114:223–232

Arbellay E, Stoffel M, Sutherland EK, Smith KT, Falk DA (2014b) Resin duct size and density as ecophysiological traits in fire scars of *Pseudotsuga menziesii* and *Larix occidentalis*. Ann Bot 114(5):973–980

Atkinson PM, Lewis P (2000) Geostatistical classification for remote sensing: an introduction. Comput Geosci 26:361–371

Ballesteros JA, Stoffel M, Bodoque JM, Bollschweiler M, Hitz OM, Díez-Herrero A (2010a) Changes in wood anatomy in tree rings of *Pinus pinaster* Ait. following wounding by flash floods. Tree-Ring Res 66(2):93–103

Ballesteros JA, Stoffel M, Bollschweiler M, Bodoque JM, Díez-Herrero A (2010b) Flash-flood impacts cause changes in wood anatomy of *Alnus glutinosa*, *Fraxinus angustifolia* and *Quercus pyrenaica*. Tree Physiol 30:773–781

Ballesteros JA, Bodoque JM, Díez A, Sanchez-Silva M, Stoffel M (2011a) Calibration of floodplain roughness and estimation of palaeoflood discharge based on tree-ring evidence and hydraulic modelling. J Hydrol 403:103–115

Ballesteros JA, Eguibar M, Bodoque JM, Díez A, Stoffel M, Gutiérrez I (2011b) Estimating flash flood discharge in an ungauged mountain catchment with 2D hydraulic models and dendrogeomorphic paleostage indicators. Hydrol Process 25:970–979

Baum S, Schwarze FWMR (2002) Large-leaved lime (*Tilia platyphyllos*) has a low ability to compartmentalize decay fungi via reaction zone formation. New Phytol 154:481–490

Bill J, Daly A, Johnsen O, Dalen KS (2012) DendroCT—dendrochronology without damage. Dendrochronologia 30:223–230

Boddy L (1992) Microenvironmental aspects of xylem defenses to wood decay fungi. In: Blanchette RA, Biggs AR (eds) Defense mechanisms of woody plants against fungi. Springer- Verlag, Berlin, pp 96–132

Boddy L, Rayner ADM (1983) Origins of decay in living deciduous trees: the role of moisture content and a re-appraisal of the expanded concept of tree decay. New Phytol 94:623–641

Bollschweiler M, Stoffel M (2010) Tree rings and debris flows: recent developments, future directions. Prog Phys Geogr 34:625–645

Bollschweiler M, Stoffel M, Schneuwly DM, Bourqui K (2008) Traumatic resin ducts in *Larix decidua* stems impacted by debris flows. Tree Physiol 28:255–263

Bucur V (2003) Non-destructive characterization and imaging of wood. Springer, Berlin

Cressie N (1992) Statistics for spatial data. Terra Nova 4:613–617

Deflorio G, Fink S, Schwarze FWMR (2008) Detection of incipient decay in tree stems with sonic tomography after wounding and fungal inoculation. Wood Sci Technol 42:117–132

Dekhuijzen HM (1976) Endogenous, cytokines in healthy and diseased plants. Encycl plant physiol. New Ser 4:526–559

Dujesiefken D, Liese W, Shortle W, Minocha R (2005) Response of beech and oaks to wounds made at different times of the year. Eur J For Res 124:113–117

Fonti P, Heller O, Cherubini P, Rigling A, Arend M (2012) Wood anatomical responses of oak saplings exposed to air warming and soil drought. Plant Biol. doi:10.1111/j.1438-8677.2012.00599.x

Freyburger C, Longuetaud F, Mothe F, Constant T, Leban J (2009) Measuring wood density by means of X-ray computer tomography. Ann For Sci 66:804

Fromm JH, Sautter I, Matthies D, Kremer J, Schumacher P, Ganter C (2001) Xylem water content and wood density in spruce and oak trees detected by high-resolution computed tomography. Plant Physiol 127:416–425

Grünwald C, Ruel K, Schmitt U (2002) Differentiation of xylem cells in rolC transgenic aspen trees—a study of secondary cell wall development. Ann For Sci 59:679–685

Guardiola-Albert C, Ballesteros-Cánovas JA, Stoffel M, Díez-Herrero A (2015) How to improve dendrogeomorphological sampling: variogram analyses of wood density using XRCT. Tree-Ring Res 71(1):25–36

Haavik LJ, Stephen FM (2011) Factors that affect compartmentalization and wound closure of *Quercus rubra* infested with *Enaphalodes rufulus*. Agric For Entomol 13:291–300

Hacke UG, Sperry JS, Pockman WT, Davis SD, McCulloh KA (2001) Trends in wood density and structure are linked to prevention of xylem implosion by negative pressure. Oecologia 126:457–461

Hacke UG, Sperry JS, Wheele JK, Castro L (2006) Scaling of angiosperm xylem structure with safety and efficiency. Tree Physiol 26:689–701

Journel AG, Huijbregts CJ (1978) Mining geostatistics. Academic Press, London

Jupp DLB, Strahler AH, Woodcock CE (1988) Autocorrelation and regularization in digital images. I. Basic theory. Geoscience and remote sesing. IEEE Trans Remote Sens 26((4):463–473

Kames S, Tardif JC, Bergeron Y (2011) Anomalous earlywood vessel lumen area in black ash (*Fraxinus nigra* Marsh.) tree rings as a potential indicator of forest fires. Dendrochronologia 29:09–114

Kogelnig-Mayer B, Stoffel M, Schneuwly-Bollschweiler M (2013) Four-dimensional growth response of mature *Larix decidua* to stem burial under natural conditions. Trees Struct Funct 27:1217–1223

Kozlowski TT (1971) The growth and development of trees. Academic Press, New York

Kozlowski TT (1997) Responses of woody plants to flooding and salinity. Tree Physiol (Monogr) 1:1–29

Kuroda K (1986) Wound effects on cytodifferentiation in the secondary xylem of woody plants. Wood Res 72:67–118

Leban JM, Pizzi A, Wieland S, Zanetti M, Properzi M, Pichelin E (2004) X-Ray microdensitometry analysis of vibration-welded wood. J Adhes Sci Technol 18:673–685

Lev-Yadun S, Aloni R (1993) Effect of wounding on the relations between vascular rays and vessels in *Melia azedarach* L. New Phytol 124:339–344

Longuetaud F, Saint-André L, Leban J (2005) Automatic detection of annual growth units on *Picea abies* logs using optical and x-ray techniques. J Nondestruct Eval 24(1):29–43

Lowerts GA, Kellison RC (1981) Genetically controlled resistance to discoloration and decay in wounded tree of yellow-poplar. Silvae Genet 30:98–101

Ma YZ, Jones TA (2001) Teacher's aide: modeling hole-effect variograms of lithology indicator variables. Math Geosci 33:631–648

Meincken M, du Plessis A (2013) Visualizing and quantifying thermal degradation of wood by computed tomography. Europ J Wood Products 71(3):387–389

Neely D (1988) Wound closure rates on trees. J Arboric 14:250–254

Pearce RB (2000) Decay development and its restriction in trees. J Arboric 26(1):1–10

Pearce RB, Fisher BJ, Carpenter TA, Hall LD (1997) Water distribution in fungal lesions in the wood of sycamore, *Acer pseudoplatanus*, determined gravimetrically and using nuclear magnetic resonance imaging. New Phytol 135:675–688

Rademacher P, Bauch J, Shigo AL (1984) Characteristics of xylem formed after wounding in Acer, Betula and Fagus. IAWA Bull 5:141–151

Rayner ADM (1986) Water and the origins of decay in trees. In: Ayres PG, Boddy L (eds) Water, fungi and plants. Cambridge University Press, Cambridge, pp 321–341

Reymond P, Weber H, Damond M, Farmer EE (2000) Differential gene expression in response to mechanical wounding and insect feeding in Arabidopsis. Plant Cell 12:707–720

Rier JP, Shigo AL (1972) Some changes in red maple, *Acer rubrum*, tissues within 34 days after wounding in July. Can J Bot 50:1783–1784

Romero C, Bolker BM, Edwards CE (2009) Stem responses to damage: the evolutionary ecology of *Quercus* species in contrasting fire regimes. New Phytol 182:261–271

Schneuwly DM, Stoffel M, Bollschweiler M (2009a) Formation and spread of callus tissue and tangential rows of resin ducts in *Larix decidua* and *Picea abies* following rockfall impacts. Tree Physiol 29:281–289

Schneuwly DM, Stoffel M, Dorren LKA, Berger F (2009b) Three-dimensional analysis of the anatomical growth response of European conifers to mechanical disturbance. Tree Physiol 29:1247–1257

Schneuwly-Bollschweiler M, Schneuwly D (2012) How fast do European conifers overgrow wounds inflicted by rockfall? Tree Physiol 32(8):968–975

Schwarze FWMR, Baum S (2000) Mechanisms of reaction zone penetration by decay fungi in wood of beech (*Fagus sylvatica*). New Phytol 146(1):129–140

Schweingruber FH (2007) Wood structure and environment. Springer, Berlin

Schweingruber FH, Börner A, Schulze ED (2006) Atlas of woody plant stems evolution, structure, and environmental modifications. Springer, Berlin

Shigo AL (1984) Compartmentalization: a conceptual framework for understanding how trees grow and defend themselves. Annu Rev Phytopathol 22:189–214

Sigafoos RS (1964) Botanical evidence of floods and flood-plain deposition. Geol Surv Prof Pap (US) 485-A:1–35

Smith KT, Sutherland EK (2001) Terminology and biology of fire scars in selected central hardwoods. Tree-Ring Res 57(2):141–147

Stobbe H, Schmitt U, Eckstein D, Dujesiefken D (2002) Developmental stages and fine structure of surface callus formed after debarking of living lime trees (*Tilia* sp.). Ann Bot 89(6):773–782

Stoffel M (2008) Dating past geomorphic processes with tangential rows of traumatic resin ducts. Dendrochronologia 26(1):53–60

Stoffel M, Corona C (2014) Dendroecological dating of geomorphic disturbance in trees. Tree-Ring Res 70:3–20

Stoffel M, Hitz OM (2008) Snow avalanche and rockfall impacts leave different anatomical signatures in tree rings of Larix decidua. Tree Physiol 28(11):1713–1720

Stoffel M, Klinkmüller M (2013) Three-dimensional analysis of wound reactions in European conifers after mechanical stem wounding: qualitative insights from X-ray computed tomography. Trees Struc Func 27:1805–1811

Stoffel M, Wilford DJ (2012) Hydrogeomorphic processes and vegetation: disturbance, process histories, dependencies and interactions. Earth Surf Process Land 37:9–22

Stoffel M, Bollschweiler M, Butler DR, Luckman BH (2010) Tree rings and natural hazards: a state-of-the-art. Springer, Berlin

Stoffel M, Butler DR, Corona C (2013) Mass movements and tree rings: a guide to dendrogeomorphic field sampling and dating. Geomorphology 200:106–120

Trappmann D, Stoffel M (2012) Counting scars on tree stems to assess rockfall hazards: a low effort approach, but how reliable? Geomorphology 180–181:180–186

Trappmann D, Corona C, Stoffel M (2013) Rolling stones and tree rings: a state of research on dendrogeomorphic reconstructions of rockfall. Prog Phys Geog 37(5):701–716

Zimmermann MH (1983) Xylem structure and the ascent of sap. Springer, Berlin